

# High-quality thin film growth of the weak topological insulator BiSe on Si (111) substrates via pulsed laser deposition

Cite as: J. Appl. Phys. **133**, 074401 (2023); <https://doi.org/10.1063/5.0130066>

Submitted: 22 October 2022 • Accepted: 29 January 2023 • Published Online: 21 February 2023

 Kunjalata Majhi,  Vivek K. Manu,  R. Ganesan, et al.



View Online



Export Citation



CrossMark

## ARTICLES YOU MAY BE INTERESTED IN

[Perspective on functional metal-oxide plasmonic metastructures](#)

Journal of Applied Physics **133**, 070901 (2023); <https://doi.org/10.1063/5.0134141>

[A review of electrochemical glucose sensing based on transition metal phosphides](#)

Journal of Applied Physics **133**, 070702 (2023); <https://doi.org/10.1063/5.0111591>

[Asymmetric acoustic metagrating enabled by parity-time symmetry](#)

Journal of Applied Physics **133**, 074504 (2023); <https://doi.org/10.1063/5.0136825>



Time to get excited.  
Lock-in Amplifiers – from DC to 8.5 GHz

[Find out more](#)

 Zurich  
Instruments

# High-quality thin film growth of the weak topological insulator BiSe on Si (111) substrates via pulsed laser deposition

Cite as: J. Appl. Phys. 133, 074401 (2023); doi: 10.1063/5.0130066

Submitted: 22 October 2022 · Accepted: 29 January 2023 ·

Published Online: 21 February 2023



Kunjalata Majhi,<sup>1</sup>  Vivek K. Manu,<sup>1,2</sup>  R. Ganesan,<sup>1</sup>  and P. S. Anil Kumar<sup>1,3,a)</sup> 

## AFFILIATIONS

<sup>1</sup>Department of Physics, Indian Institute of Science, Bangalore 560012, India

<sup>2</sup>Department of Physics, The University of Texas at Dallas, Richardson, Texas 75080-3021, USA

<sup>3</sup>Centre for Nanoscience and Engineering, Indian Institute of Science, Bangalore 560012, India

<sup>a)</sup>Author to whom correspondence should be addressed: [anil@iisc.ac.in](mailto:anil@iisc.ac.in)

## ABSTRACT

In this work, we report the growth of high-quality BiSe thin films deposited on Si (111) substrates at different temperatures via pulsed laser deposition. We observe poor sample quality at a low substrate temperature ( $T_{sub} = 175^\circ\text{C}$ ), and as the substrate temperature increases, the crystallinity of the samples increases. At a substrate temperature,  $T_{sub} = 250^\circ\text{C}$ , BiSe Raman modes (modes centered around  $97.6$  and  $112.9\text{ cm}^{-1}$ ) start to emerge with less intensity and evolve with the increase in the substrate temperature and at  $T_{sub} = 325^\circ\text{C}$  closely match with that of single crystals. These modes correspond to the vibrations of Se-atoms from the  $\text{Bi}_2\text{Se}_3$  quintuple layers and Bi-atoms from the Bi-bilayer. By carefully investigating the structural properties and the Raman modes of BiSe thin films at each substrate temperature, we provide an optimal condition to grow high-quality thin films of BiSe by pulsed laser deposition.

Published under an exclusive license by AIP Publishing. <https://doi.org/10.1063/5.0130066>

## INTRODUCTION

The discovery of topological insulators has generated a tremendous amount of interest in the field of condensed matter physics due to its exotic surface states, thereby making itself a promising candidate for potential applications in spintronics and quantum computation.<sup>1–3</sup> The weak topological insulators (WTIs) are less explored unlike its counterpart strong topological insulators (STIs) both theoretically as well as experimentally.<sup>4–6</sup> Even though a few of WTIs have been materialized,<sup>7,8</sup> the difficulties in their synthesis process and the lack of high-quality samples hinder the progress in understanding this phase further.<sup>7,9</sup> Recently discovered BiSe with an indirect bandgap of  $50\text{ meV}$  provides an excellent platform to understand this phase in detail due to its cleavability nature; however, cleaving does not give control over thickness.<sup>10</sup> Apart from that, it has also been a challenge to access the surface states due to the presence of high bulk carriers because of defects and Se-deficiencies. The most efficient way to solve these problems would be to grow thin films that reduce the bulk carrier density by increasing the surface-to-volume ratio and also gives control over thickness. Here, we present an optimal condition to grow

high-quality thin films of BiSe by pulsed laser deposition (PLD). Previously, thin films of topological insulators have been grown on Si(111) successfully and have shown the desirable topological properties.<sup>11–13</sup> Here, thin films of BiSe were deposited on Si (111) substrates at temperatures ranging from  $175^\circ\text{C}$  to  $325^\circ\text{C}$  (S1-S7) with an interval of  $25^\circ\text{C}$ . The thin films are then characterized by basic characterization techniques such as x-ray diffraction, atomic force microscopy, and Raman measurements to probe the growth quality at each substrate temperature to obtain high-quality thin films of BiSe. High-quality single crystal bulk of BiSe grown by Bridgman technique is used to benchmark the thin film samples studied in this paper.

## EXPERIMENTAL DETAILS

Each unit cell of BiSe consists of a double layer of Bi sandwiched between two  $\text{Bi}_2\text{Se}_3$  layers where the Bi–Bi are held by covalent bonds and  $\text{Bi}_2\text{Se}_3 - \text{Bi}_2\text{Se}_3$  in adjacent unit cells by van der Waal forces. It crystallizes in trigonal symmetry belonging to the space group of P-3ml.<sup>14</sup> The lattice constants of BiSe are  $a = 4.212\text{Å}$ ,  $b = 4.212\text{Å}$ , and  $c = 22.94\text{Å}$ . Thin films of BiSe were deposited on Si (111)

substrates via the PLD method under high vacuum ( $10^{-5}$  mbar). The target for PLD was prepared from Bi (99.999%) and Se (99.99%) elements of high purity. Considering the high vapour pressure of Se, we have taken 50% of excess Se to get the BiSe stoichiometry. The substrates are cleaned with absolute care prior to deposition with acetone to remove the dirt particles, followed by isopropyl alcohol and DI water. The substrates were then dipped in hydrochloric acid to strip the oxide layer. Thin films were deposited at substrate temperatures ranging from 150 °C to 325 °C with an interval of 25 °C. The substrate temperature plays an important role in the growth process of thin films. It controls the kinetics, rate of reaction, and the quality and the final composition of the thin films.<sup>15</sup> At a low substrate temperature, the adatoms do not have enough energy to move around the substrate to find the lowest potential site, thus leading to amorphous or polycrystalline films. On the other hand, if the substrate temperature is too high, different island-type growths are seen, and at very high temperatures, films do not form due to the low sticking co-efficient of the adatoms on the substrates.<sup>15</sup> We did not obtain any film at 350 °C. The laser parameters were optimized to obtain films of similar thicknesses. The pulses were fired at 20 Hz frequency with an energy of 31 mJ. The thickness of the films studied in this report is  $20 \pm 3$  nm.

## RESULTS AND DISCUSSION

We employed the x-ray diffraction method to identify the phase formation and the degree of crystallinity. X-ray diffraction patterns were recorded by a Bruker D8 diffractometer and monochromatic  $\text{CuK}\alpha$  radiation of wavelength 1.5418 Å was used as the x-ray source. Figure 1(a) shows XRD patterns taken on thin film samples, S1–S7, deposited at different substrate temperatures. We observe that with the increase in the substrate temperature, the quality of the films improves and becomes highly oriented along

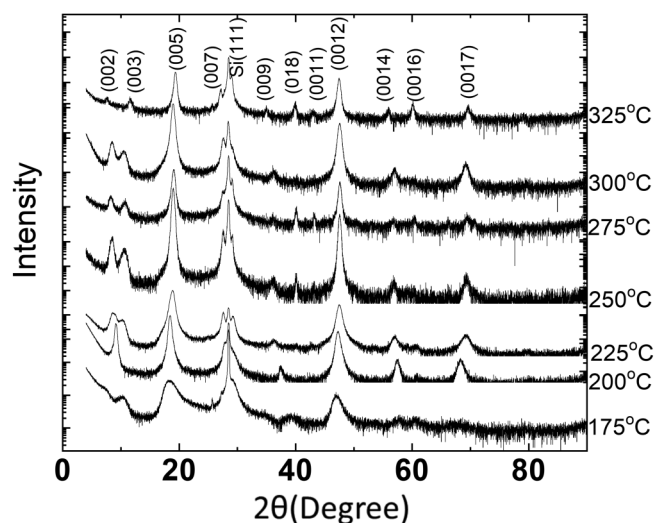


FIG. 1. X-ray diffraction patterns of thin films grown at different substrate temperatures.

the c-axis according to standard ICSD data. Although the BiSe phase starts forming from 250 °C(S4) onwards, better quality is attained as explained by Fig. 1. A FWHM analysis carried out on the (005) peak shows the improvement in crystallinity as the substrate temperature increases. The data from sample S7 showed the best match to the standard ICSD XRD data of BiSe along with the lowest value of FWHM of the (005) peak.

The surface morphology/topography of thin films was investigated using tapping mode atomic force microscopy (AFM) with Bruker's AFM Dimension ICON Sys1, and the analysis was carried out using Nanoscope Analysis software. All the measurements were carried out at room temperature. An AFM analysis is used to measure quantitatively the nanometric dimensional surface roughness and to visualize the surface nano-texture of the deposited thin films. The surface roughness of conductive thin films significantly influences device performance.<sup>16</sup> Figures 2(a)–2(h) show the AFM image of thin film samples grown at different temperatures, i.e., from 175 to 325 °C scanned over an area of 500 nm<sup>2</sup>. With the increase in the substrate temperature, it is observed that the growth pattern changes from island to triangular type. At 175 °C, the growth pattern is island type, with an island height of > 2 nm and the grain size of ~50 nm. As we increase the substrate temperature to 200 °C, the island-type growth continues but with smaller island heights and grain size. The growth pattern slowly changes to the columnar-type as we further increase the substrate temperature to 230 °C. From temperature 250 °C onward, we observed big-sized arbitrary shaped grain formation until 300 °C. At 325 °C, the films grow in a triangular fashion, as seen from the images (marked in white color). Above 325 °C, we did not obtain films.<sup>15</sup> The triangular growth refers to the high-quality of the films and has been known to provide a good platform for electrical transport measurements.<sup>16</sup>

All the Raman measurements were carried out using the LabRam HR system at room temperature in a controlled environment. The wavelength of laser light used was 532 nm with a beam size of 0.15 μm. All the spectra were recorded in a back-scattering geometry and showed only Stoke's transitions. The Raman spectra of all the films showed the standard, e.g.,  $A_{1g}$ -,  $E_g$ - symmetry modes that are commonly observed in Bi-based chalcogenide materials. The  $A_{1g}$ - and  $E_g$ -symmetry modes correspond to out-of-plane (non-degenerate modes) and in-plane (double degenerate modes) vibrations of Bi–Se pairs [see Fig. 3(b)]

Figure 3 shows the Raman spectra of thin films of BiSe deposited at different substrate temperatures. A Raman spectrum of the single crystal data has been attached along with the thin films for a better comparison. Samples S1–S3 show the presence of three modes, e.g.,  $A_{1g}^1$ ,  $E_g^2$ , and  $A_{1g}^4$  that has been commonly observed in Bi-based topological insulators.<sup>17–22</sup> Interestingly, from sample S4 onward, two new modes centered around 97.6 and 112.9  $\text{cm}^{-1}$  emerge in the Raman spectra [indicated in small black arrows in Fig. 3(a)].

The new modes are recognized to be  $E_g^1$  and  $A_{1g}^2$ , which correspond to the vibrations of Se-atoms from the  $\text{Bi}_2\text{Se}_3$  quintuple layers and Bi- atoms from the Bi-bilayer. The intensity of these two new modes is found to increase as we increase the substrate temperature. The peak intensity of a mode reflects the concentration of the molecules having a particular vibration or the density of a particular vibrational state. The appearance of such modes provide information about the gradual formation of BiSe.

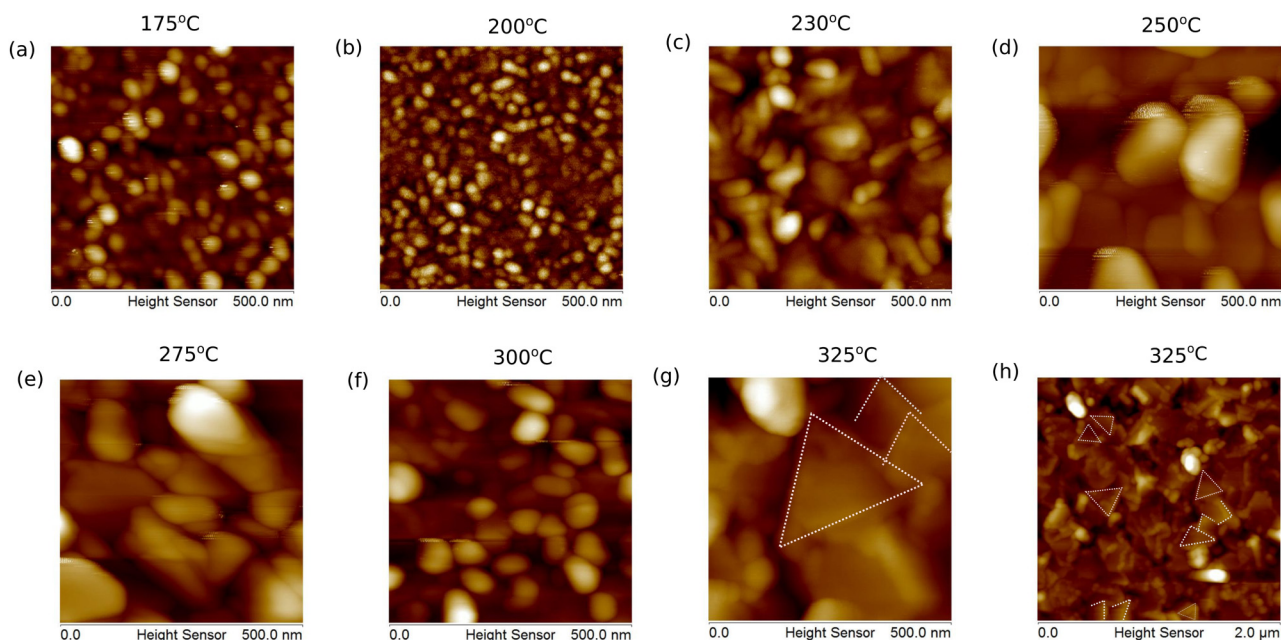


**FIG. 2.** AFM images of thin film samples grown at different substrate temperatures. The substrate temperatures are mentioned on the top of the AFM images. (a) and (b) AFM images show the granular growth pattern of the samples, (c)–(f) show island-type growth of the samples, and (g) and (h) show the triangular growth of the samples.

The Raman spectrum from a single crystal flake has been included in the data to compare it with our observed thin film spectra and placed as single crystal in the x-axis. The compositional analysis carried out on the single crystals of BiSe produces an

empirical formula  $\text{Bi}_1\text{Se}_1$ . All the five modes, i.e.,  $A_{1g}^1, A_{1g}^2, E_g^1, E_g^2$ , and  $A_{1g}^4$ , show red shift with respect to the substrate temperature. From sample S5 to S6, a crucial shift is observed toward the formation of a high-quality thin film in accordance with the single crystal

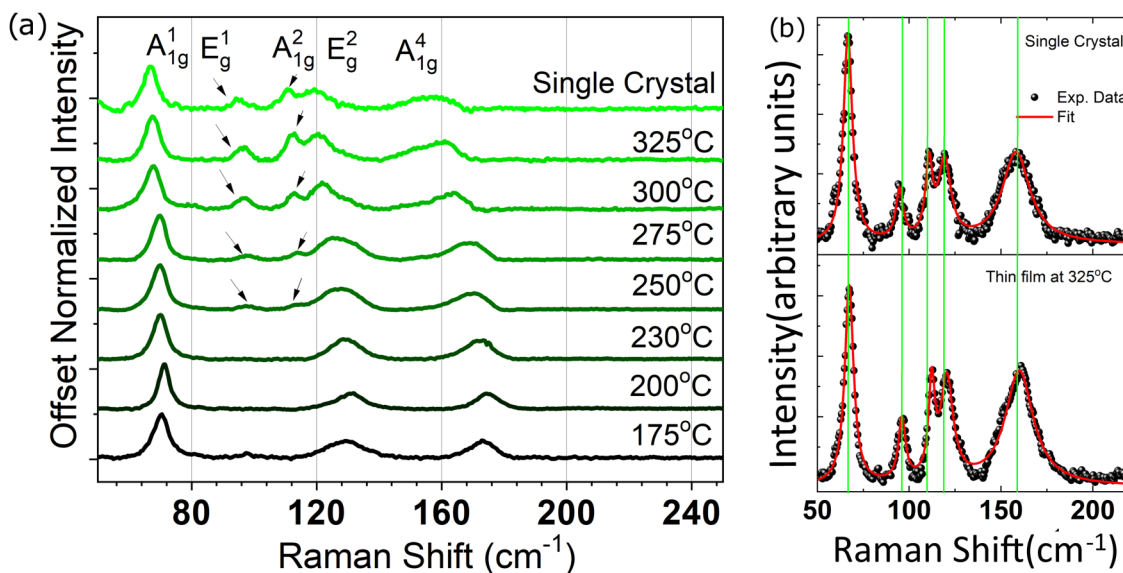


**FIG. 3.** Raman measurements on thin films of BiSe (a) shows Raman spectra of thin films grown at different substrate temperatures and (b) shows a fit to the experimental data for a single crystal and a thin film grown at 325 °C.

**TABLE I.** Evolution of Raman modes with respect to substrate temperature. The optimum grown film as well as single crystal data are highlighted.

Temp °C	$A_{1g}^1$	$E_g^1$	$A_{1g}^2$	$E_g^2$	$A_{1g}^4$
S <sub>175</sub>	70.2	x	x	128.1	173.1
S <sub>200</sub>	71.0	x	x	129.2	174.9
S <sub>230</sub>	69.9	x	x	129.0	171.8
S <sub>250</sub>	69.6	97.4	112.6	127.6	169.5
S <sub>275</sub>	67.5	97.7	113.0	126.8	168.6
S <sub>300</sub>	67.4	96.4	112.2	121.9	162.5
S <sub>325</sub>	67.3	96.2	112.1	120.6	159.5
SC	67.0	95.0	110.7	119.3	156.0

data. It is observed that sample S7 shows a good match with that of the single crystal Raman modes with nearly identical peak positions and relative intensities. Table I details the Raman modes and their corresponding peak positions at different substrate temperatures.

Careful peak fitting analysis has been carried out on all the peaks using Lorentzian line shapes as shown in Fig. 3(b). The area of the peak has been used for fitting as it is a better indicator of concentration and absorption because the final peak profile is a sum of all the individual elements. In some cases, there is a possibility of change in peak height due to the broadening mechanism, but the area remains the same as the number of molecules is constant. Figure 4 shows the change in peak positions and FWHM of the Raman modes. The modes  $A_{1g}^1$ ,  $E_g^1$ , and  $A_{1g}^2$  differ by a slight change in frequency by 3.2, 2.4, and 1.9  $\text{cm}^{-1}$  from the initial growth temperature, whereas  $E_g^2$  and  $A_{1g}^4$  modes differ significantly in frequency (see Table I). The most striking feature is that at 325 °C the Raman modes of the thin films closely match with the Raman modes of single crystal data including the FWHM values. The FWHM of the Raman spectra fitted with Lorentzian line shape

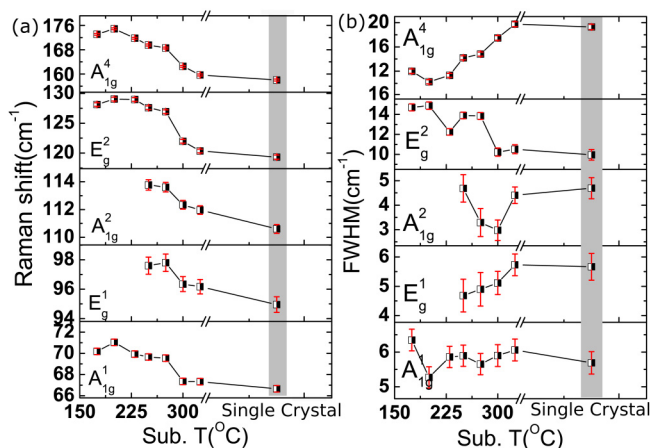


**FIG. 4.** Analysis of the Raman modes: (a) The variation of peak positions and (b) FWHM at different substrate temperatures indicating that the peak positions of the thin films approach the single crystal data with the increase in substrate temperature.

is found to be remaining almost constant for  $A_{1g}^1$ ,  $E_g^1$ , and  $A_{1g}^2$  modes but shows significant broadening for  $E_g^2$  and  $A_{1g}^4$  modes as can be seen from Fig. 4(b).

## CONCLUSION

Here, we provide an optimal growth condition to grow high-quality thin films of weak topological insulator BiSe on Si(111) substrates. We have used PLD to grow thin films of BiSe and employed some basic material characterization techniques such as x-ray diffraction, atomic force microscopy, and Raman spectroscopy to study the gradual formation of BiSe at each substrate temperature. We check the crystallinity of the samples from x-ray diffraction, evolution of growth pattern from granular to triangular from AFM characterization, and in Raman measurements, we see the gradual evolution of Raman modes of BiSe thin films with the increase in the substrate temperature. At a substrate temperature,  $T_{sub} = 250$  °C, BiSe Raman modes (modes centered around 97.6 and 112.9  $\text{cm}^{-1}$ ) start to emerge with less intensity and evolve with the increase in the substrate temperature and at  $T_{sub} = 325$  °C closely match with that of single crystals. These modes correspond to the vibrations of Se-atoms from the  $\text{Bi}_2\text{Se}_3$  quintuple layers and Bi-atoms from the Bi-bilayer. The observed Raman modes match with the theoretical Raman modes calculated by DFT at room temperature, and at the optimum temperature, all the Raman modes match with that of single crystal modes implying the high quality of the samples.

## ACKNOWLEDGMENTS

K.M. acknowledge CSIR India for financial support. P.S.A.K. acknowledge Nanomission DST government of India for financial support.

## AUTHOR DECLARATIONS

### Conflict of Interest

The authors have no conflicts to disclose.

### Author Contributions

**Kunjalata Majhi:** Conceptualization (equal); Data curation (equal); Formal analysis (equal); Investigation (equal); Writing – original draft (equal). **Vivek K. Manu:** Conceptualization (equal); Data curation (supporting); Formal analysis (supporting); Investigation (supporting); Methodology (equal); Writing – review & editing (supporting). **R. Ganesan:** Project administration (equal); Resources (equal); Supervision (equal); Writing – review & editing (equal). **P. S. Anil Kumar:** Conceptualization (equal); Funding acquisition (lead); Project administration (lead); Resources (lead); Supervision (lead); Writing – review & editing (lead).

## DATA AVAILABILITY

The data that support the findings of this study are available from the corresponding author upon reasonable request.

## REFERENCES

- <sup>1</sup>M. Z. Hasan and C. L. Kane, "Colloquium: Topological insulators," *Rev. Mod. Phys.* **82**, 3045–3067 (2010).
- <sup>2</sup>L. Fu, C. L. Kane, and E. J. Mele, "Topological insulators in three dimensions," *Phys. Rev. Lett.* **98**, 106803 (2007).
- <sup>3</sup>J. E. Moore and L. Balents, "Topological invariants of time-reversal-invariant band structures," *Phys. Rev. B* **75**, 121306 (2007).
- <sup>4</sup>Z. Ringel, Y. E. Kraus, and A. Stern, "Strong side of weak topological insulators," *Phys. Rev. B* **86**, 045102 (2012).
- <sup>5</sup>K.-I. Imura, Y. Takane, and A. Tanaka, "Weak topological insulator with protected gapless helical states," *Phys. Rev. B* **84**, 035443 (2011).
- <sup>6</sup>T. Morimoto and A. Furusaki, "Stability of surface states of weak  $Z_2$  topological insulators and superconductors," *Phys. Rev. B* **89**, 035117 (2014).
- <sup>7</sup>B. Rasche, A. Isaeva, M. Ruck, S. Borisenko, V. Zabolotnyy, B. Büchner, K. Koepernik, C. Ortix, M. Richter, and J. V. D. Brink, "Stacked topological insulator built from bismuth-based graphene sheet analogues," *Nat. Mater.* **12**, 422–425 (2013).
- <sup>8</sup>X.-B. Li, W.-K. Huang, Y.-Y. Lv, K.-W. Zhang, C.-L. Yang, B.-B. Zhang, Y. B. Chen, S.-H. Yao, J. Zhou, M.-H. Lu, L. Sheng, S.-C. Li, J.-F. Jia, Q.-K. Xue, Y.-F. Chen, and D.-Y. Xing, "Experimental observation of topological edge states at the surface step edge of the topological insulator  $ZrTe_5$ ," *Phys. Rev. Lett.* **116**, 176803 (2016).
- <sup>9</sup>G. Yang, J. Liu, L. Fu, W. Duan, and C. Liu, "Weak topological insulators in  $PbTe/SnTe$  superlattices," *Phys. Rev. B* **89**, 085312 (2013).
- <sup>10</sup>K. Majhi, K. Pal, H. Lohani, A. Banerjee, P. Mishra, A. K. Yadav, R. Ganesan, B. R. Sekhar, U. V. Waghmare, and P. S. Anil, "Kumar emergence of a weak topological insulator from the  $BixSe_y$  family," *Appl. Phys. Lett.* **110**, 162102 (2017).
- <sup>11</sup>N. Bansal, Y. S. Kim, E. Edrey, M. Brahlek, Y. Horibe, K. Iida, M. Tanimura, G.-H. Li, T. Feng, H.-D. Lee, T. Gustafsson, E. Andrei, and S. Oh, "Epitaxial growth of topological insulator  $Bi_2Se_3$  film on  $Si(111)$  with atomically sharp interface," *Thin Solid Films* **520**, 224–229 (2011).
- <sup>12</sup>S. X. Zhang, L. Yan, J. Qi, M. Zhuo, Y.-Q. Wang, R. P. Prasan kumar, Q. X. Jia, and S. T. Picraux, "Epitaxial thin films of topological insulator  $Bi_2Te_3$  with two-dimensional weak anti-localization effect grown by pulsed laser deposition," *Thin Solid Films* **520**, 6459–6462 (2012).
- <sup>13</sup>G. Zhang, H. Qin, J. Teng, J. Guo, Q. Guo, X. Dai, Z. Fang, and K. Wua, "Quintuple-layer epitaxy of thin films of topological insulator  $Bi_2Se_3$ ," *Appl. Phys. Lett.* **95**, 053114 (2009).
- <sup>14</sup>E. Gaudin, S. Jobic, M. Evain, R. Brec, and J. Rouxel, "Charge balance in some  $Bi_xSe_y$  phases through atomic structure determination and band structure calculations," *Mater. Res. Bull.* **30**, 549 (1995).
- <sup>15</sup>A. Mzard, D. Sayah, J. C. Tedenac, and A. Boyer, "Optimal crystal growth conditions of thin films of  $Bi_2Te_3$  semiconductors," *J. Cryst. Growth* **140**(3–4), 365 (1994).
- <sup>16</sup>G. Zhang, H. Qin, J. Chen, X. He, L. Lu, Y. Li, and K. Wu, "Growth of topological insulator  $Bi_2Se_3$  thin films on  $SrTiO_3$  with large tunability in chemical potential," *Adv. Funct. Mater.* **21**, 2351–2355 (2011).
- <sup>17</sup>W. Richter and C. R. Becker, "A Raman and far-infrared investigation of phonons in the rhombohedral  $V_2-VI_3$  compounds  $Bi_2Te_3$ ,  $Bi_2Se_3$ ,  $Sb_2Te_3$  and  $Bi_2(Te_{1-x}Se_x)_3$  ( $0 < x < 1$ ),  $(Bi_{1-y}Sb_y)_2Te_3$  ( $0 < y < 1$ )," *Phys. Status Solidi B* **84**, 619 (1977).
- <sup>18</sup>V. Chis, I. Y. Sklyadneva, K. A. Kokh, V. A. Volodin, O. E. Tereshchenko, and E. V. Chulkov, "Vibrations in binary and ternary topological insulators: First principles calculations and Raman spectroscopy measurements," *Phys. Rev. B* **86**, 174304 (2012).
- <sup>19</sup>J. Yuan, M. Zhao, W. Yu, Y. Lu, C. Chen, M. Xu, S. Li, K. P. Loh, and Q. Bao Raman, "Spectroscopy of two-dimensional  $Bi_2Te_xSe_{3-x}$  platelets produced by Solvothermal method," *Materials* **8**, 5007–5017 (2015).
- <sup>20</sup>J. Zhang, Z. Peng, A. Soni, Y. Zhao, Y. Xiong, B. Peng, J. Wang, M. Dresselhaus, and Q. S. Xiong, "Raman spectroscopy of few-quintuple layer topological insulator  $Bi_2Se_3$  nanoplatelets," *Nano Lett.* **11**, 2407–2414 (2011).
- <sup>21</sup>K. M. F. M. Shahil, Z. Hossain, V. Goyal, and A. A. Balandin, "Micro-Raman spectroscopy of mechanically exfoliated few-quintuple layers of  $Bi_2Te_3$ ,  $Bi_2Se_3$ , and  $Sb_2Te_3$  materials," *J. Appl. Phys.* **111**(5), 054305 (2012).
- <sup>22</sup>H.-H. Kung, M. Salehi, I. Boulares, A. F. Kemper, N. Koirala, M. Brahlek, P. Lošťák, C. Uher, R. Merlin, X. Wang, S.-W. Cheong, S. Oh, and G. Blumberg, "Surface vibrational modes of the topological insulator  $Bi_2Se_3$  observed by Raman spectroscopy," *Phys. Rev. B* **95**, 245406 (2017).